# A Review of Time Domain Methods for Fatigue and Damage Estimation

Pierre Lague

[1] Inria, Rennes (France)

June 5, 2026

**Abstract**

Time-domain fatigue methods represent the foundational approach to structural durability assessment, operating directly on stress or strain histories to extract damaging cycles and predict component life. Unlike frequency-domain spectral techniques, time-domain approaches explicitly resolve load sequences, making them the natural choice for non-stationary, non-Gaussian, or sequence-dependent damage mechanisms. This review surveys the evolution and current state of time-domain fatigue assessment from the pioneering work of Palmgren and Miner in the 1920s–1940s and ways of characterizing fatigue or damage in a system, through recent developments in physics-informed machine learning, real-time structural health monitoring, and nonlinear damage accumulation models.

## 1 Introduction

Fatigue damage is the progressive, localized structural deterioration that occurs when materials are subjected to repeated cyclic loading. Time-domain methods address fatigue by analyzing the complete temporal evolution of stress or strain at critical locations, explicitly accounting for every load reversal, sequence, and amplitude variation in the service history. This direct approach stands in contrast to frequency-domain spectral methods, which work with statistical representations (power spectral densities) of the loading process. For each of these approaches, the estimation of fatigue damage is a sequential process.

The time-domain approach emerged from early 20th-century metallurgical studies. Arvid Palmgren (1924) introduced the concept of linear damage accumulation for ball bearing fatigue, and Milton A. Miner (1945) generalized this into the cumulative damage hypothesis that bears their names [1, 2]. The development of reliable cycle-counting algorithms—particularly the rainflow method by Matsuishi and Endo (1968)—provided the algorithmic foundation that transformed time-domain fatigue from a conceptual framework into a practical engineering tool [3]. Today, time-domain methods remain the reference standard against which all other approaches are calibrated, serving as the "ground truth" for fatigue predictions across aerospace, automotive, offshore, and civil engineering applications [4].

The enduring relevance of time-domain methods stems from several fundamental advantages. First, they impose minimal assumptions about the loading process—no requirements for stationarity, Gaussianity, or spectral bandwidth constraints [5]. Second, they naturally accommodate sequence-dependent phenomena such as load interaction effects, crack retardation following overloads, and mean stress evolution [6, 7]. Third, they integrate seamlessly with nonlinear material models, including plasticity-based strain-life approaches and continuum damage mechanics formulations [8, 9]. Fourth, they provide cycle-by-cycle resolution that enables real-time damage tracking in structural health monitoring systems [10].

However, these advantages come at computational cost. Time-domain analysis requires complete stress or strain histories—often spanning millions of data points for long operational lifetimes—and computationally intensive cycle-counting algorithms. For structures analyzed via finite element methods at thousands of nodes, or for design optimization requiring hundreds of iterations, the cost can become prohibitive. This has motivated the parallel development of frequency-domain methods and, more recently, hybrid approaches that combine the

efficiency of spectral methods with the accuracy of time-domain reference calculations [4, 11].

The review is organized around the core pipeline of time-domain analysis: cycle identification via counting algorithms (rainflow, range-pair, level-crossing) presented in Section 3, local stress-strain approaches for different fatigue regimes (high-cycle S-N, low-cycle strain-life) presented in Section 4, and damage accumulation rules (historical linear Palmgren-Miner and modern nonlinear variants) presented in Section 5. Then we will propose in Section 6 a discussion on the complementarity between time-domain methods and frequency-domain methods, and how they build on top of each other in theory and in various application domains. After that, we will introduce in Section 7 the concepts of Maximum or Extreme Response Spectrum (MRS) and Fatigue Damage Spectrum (FDS) that are frequency-domain indicators which can be extracted with a time-domain transform to characterize the severity of vibration environments. Finally, in Section **??** we will talk about recent advances in machine learning for time-domain analysis of vibration data.

# 2 Time-Domain Approach as Reference Standard

The time-domain approach remains the benchmark for vibration-induced fatigue assessment bevause it operates directly on the measured or simulated stress/strain history. Zorman, Slavic and Boltezar (2023) [12] emphasize that "the time-domain fatigue analysis (TFDA) is aknowledged as the more precise technique for predicting random fatigue" and that all frequency-domain models are validated against TFDA results obtained from Rainflow counting [3] combined with Palmgren-Miner [1, 2] damage accumulation model.

In this workflow a structural response time series (acceleration, force or relative displacement) is first generated from the vibration excitation, either by measurement, transient dynamic simulation, or mathematically [13–15]. The signal is then decomposed into individual fatigue cycles, damage is computed for each cycle via a material S-N law [16], and the total damage is accumulated using a cumulative-damage rule. Because every peak-valley pair and its sequence are retained, TFDA captures load-sequence effects, non-Gaussian excursions and non-stationary features that frequency-domain methods must approximate.

Slavic, Mrsnik and Boltezar (2013) [4] note that TFDA "uses a technique called rainflow cycle counting to decompose a variable-amplitude time signal of stress into fatigue cycles... the damage from each cycle is then computed using an S/N curve, and the damage over the entire time signal is finally calculated by summing the damage from all the individual cycles, using, for example, the celebrated Palmgren-Miner linear damage rule". The same authors stress that TFDA is computationally demanding because it requires long time histories and many simulations to achieve statistical convergence, yet it provides the true value of fatigue life against which frequency-domain methods are judged.

Halfpenny (1999) [17] presents a parallel tutorial stating that "Fatigue damage is traditionally determined from time signals of loading, usually in the form of stress or strain. This approach is satisfactory for periodic loading but requires very large time records to accurately capture the random nature of the load". He then outlines the standard pipeline—rainflow extraction, histogram construction, S-N curve lookup and Miner summation—as the reference that frequency-domain estimators attempt to reproduce. A recent comparative review by Muniz-Calvente et al. (2022) [18] emphasizes the complementarity of time and frequency-domain methods. How they build on top of each other, and how time-domain remains the "ground truth" for newer methods.

Recent advancements in fatigue life estimation have seen a surge in novel approaches, moving beyond traditional methods. In the time domain, rainflow counting remains a cornerstone for simplifying complex load histories into stress cycles for more accurate fatigue damage assessment. However, the research is pushing towards more sophisticated damage accumulation models that can better account for the complexities of real-world loading scenarios [6, 19].

Recent research has focused on developing new models that offer higher fidelity in fatigue life prediction. For instance, S.C. Tien, et al. (2021) [20] have proposed an energy-based time derivative damage accumulation model that avoids the ambiguity of cycle-counting by tracking damage increment at every time step. This approach is particularly useful for random loading scenarios. Further refining these concepts, L. Zhang, et al. (2024) [21] have put forward a modified Damage Stress Model (DSM) that addresses the variability of ultimate stress during damage transfer, enhancing prediction accuracy.

# 3 Cycle Counting Methods

## 3.1 Early Methods

As mentioned before, cycle counting is the cornerstone operation of time-domain fatigue analysis. Real-world load histories rarely consist of simple constant-amplitude sinusoidal cycles; instead, they exhibit irregular, multi-level amplitude variations superimposed on transient and mean stress shifts. Cycle counting algorithms transform these complex histories into a discrete set of well-defined cycles, each characterized by an amplitude, mean value, and (in some formulations) sequence position. The counted cycles are then fed into damage models for life prediction.

The simplest cycle-counting approaches emerged in the 1950s and 1960s as researchers sought systematic ways to quantify fatigue damage from irregular service loads [22]. Level-crossing counting tracks how many times a stress signal crosses pre-defined threshold levels, providing a crude histogram of stress magnitudes but failing to capture cycle amplitudes or mean stresses. Peak-counting and valley-counting methods identify local maxima and minima in the stress history, pairing them according to various rules to form cycles.

Range-counting methods improved upon simple peak counts by pairing peaks with subsequent valleys to define stress ranges [23, 24]. However, these early methods suffered from a fundamental limitation: they could not properly account for nested or interrupted cycles—situations where a large stress excursion contains smaller reversals embedded within it. As a result, range-counting methods either undercounted damaging cycles (by ignoring small embedded reversals) or overcounted them (by double-counting ranges that were already part of larger cycles).

Comparative studies and industrial researchers demonstrated that these simplified counting methods could introduce errors exceeding 50% in predicted fatigue lives when applied to realistic variable-amplitude spectra encountered in aircraft, automotive, and structural applications [22, 25]. Their use today is largely relegated to historical reference or specialized cases where load histories are inherently simple.

## 3.2 Rainflow Cycle Counting: Theory and Implementation

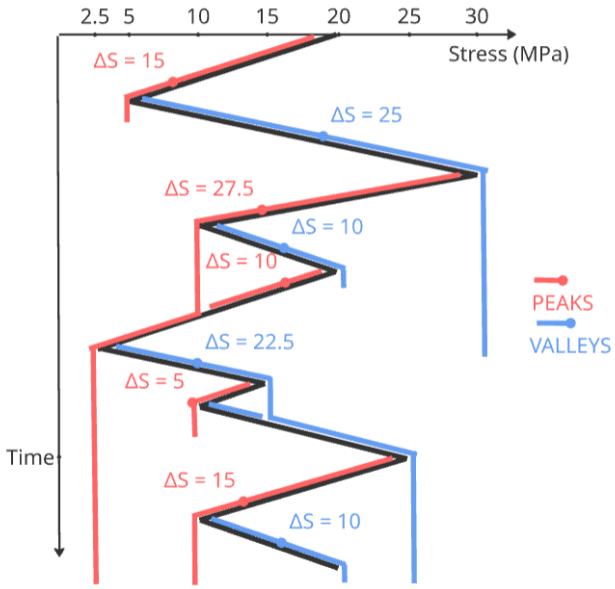


Figure 1: Illustration of the Rainflow "Pagoda roof" counting method. In red, Rainflow applied to peaks, and in blue Rainflow applied to valleys. Each half cycle (valley and peak) of same amplitude is associated to form a full cycle.

The rainflow counting algorithm, independently developed by Matsuishi and Endo in Japan (1968) [3] and popularized in the West by Dowling and Socie [26], represents the most significant methodological advance in time-domain fatigue analysis. The method derives its name from a vivid analogy: if the stress-time history is rotated 90 degrees and imagined as a pagoda roof, "rainwater" (see Figure 1) flowing down the stress peaks and

valleys follows paths that precisely identify closed hysteresis loops in the stress-strain space—the fundamental units of fatigue damage. This algorithm was formalized by Rychlik in 1987 [27] and later standardized in ASTM (American Society for Testing Materials) E1049; it remains the most accurate method for extracting fatigue-relevant cycles from arbitrary load histories [28].

Zorman et al. (2023) [12] describe the procedure succinctly: "rainflow counting... obtain[s] many stress rainflow cycles... the estimation of random fatigue life is achieved by using the amplitudes of stress cycles, material properties (S-N curves) and Miner's rule". The implementation requires a one-dimensional stress time series; the algorithm scans the signal to identify reversals, pairs peaks with corresponding valleys, and outputs a list of cycle ranges and means. The resulting cycle distribution is typically summarized in a cycle-amplitude histogram (see Figure 2) or, for variable-amplitude loading, in a rainflow matrix.

Slavic et al (2013) [4] demonstrate the practical use of rainflow counting on automotive vibration profiles: "the rainflow algorithm was used on $s(t)$ (the stress history) to extract the cycles and the probability density function of rainflow counted ranges, which in turn allowed calculating the fatigue damage for any given material constants in an S/N curve". Their study confirms that rainflow-based TDFA yields the "exact reference value" for fatigue life, which they denote as TRFC (Time-domain Rainflow Counting).

Halfpenny (1999) [17] provides a pedagogical illustration: "Each cycle will induce a certain amount of fatigue damage on the component. The total damage caused by the time history can therefore be obtained by summing the damage caused by each cycle shown in the stress range histogram. This approach is known as the Palmgren-Miner accumulated damage".

Ling (2010) [29] extends rainflow counting to stochastic characterization, combining it with Markov-chain and ARMA methods to generate statistically equivalent load spectra for Monte-Carlo fatigue simulation. Computational considerations are also discussed. Marsh (2016) [28] reviews "Rainflow residue processing techniques" that handle truncated records or very long signals, ensuring that residual half-cycles are properly accounted for to avoid bias in damage estimates.

### 3.2.1 Implementation and Interpretation

Rainflow counting is rooted in the observation that fatigue damage accumulates primarily through closed stress-strain hysteresis loops. When a material undergoes a stress cycle (loading from A to B, then unloading back toward A), it traces a hysteresis loop due to dislocation motion. The area of this loop represents dissipated energy contributing to damage. Rainflow counting identifies precisely these closed loops, even when they are embedded within more complex loading sequences [25]. In Figure 1 the loading history breaks down into a sequence of complete and half cycles that can be clearly identified by the stress reversals marked along the curve (peaks and valleys). Several full cycles appear where a peak is followed by a valley and then returns to a comparable reversal point—for example, the initial flow (red line, $\Delta S = 15$ MPa) is closed when a similar load of same amplitude occurs towards the end of the history. Smaller embedded full cycles are also visible, such as the $\Delta S = 10$ MPa cycle that occurs within the tighter zig-zag region near the middle of the plot. In addition to these complete loops, the history contains distinct half cycles associated to the maximum and minimum of the history. The highest peak will never find another peak to complete the cycle, hence the rainflow drops at the end of the plot (red line $\Delta S = 27.5$ MPa). Similarly, the lowest valley will never find a lower or equal valley to complete the cycles (blue line $\Delta S = 22.5$ MPa). Cycles that begin and never find a matching amplitude to reverse the load are marked as half-cycles.

The algorithm operates according to simple rules that can be stated algorithmically. The most common implementation, standardized in ASTM E1049-85, processes the stress-time history by identifying peaks and valleys, then applying flow rules to determine which reversals form closed cycles [30]. Crucially, the algorithm respects the sequence dependence of the loading: a small cycle embedded during the rising portion of a large cycle is counted differently than the same small cycle occurring in isolation.

Below we emphasize understanding the algorithm: what it does *and* why it works. In Appendix A, the reader will find a compact pseudocode that follows the original Matsuishi–Endo [3] logic.

**Conceptual summary**

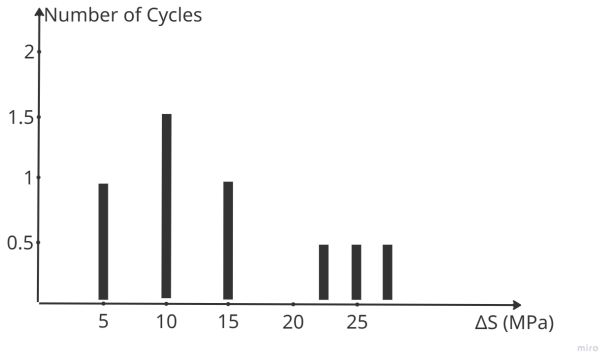


Figure 2: Cycle-Amplitude distribution extracted from the rainflow example in Figure 1. Note that the construction of this distribution has to be made over a large number of cycles to ensure statistical convergence. Frequency domain methods seek to approximate this distribution with statistical laws.

- The input is a scalar time series $s(t)$ sampled sufficiently densely. First the series is reduced to its sequence of *turning points* (local maxima and minima). Only these extrema are relevant for cycle extraction.
- Rainflow pairs peaks and valleys according to a simple local rule that emulates how water would flow down a sequence of ridges (hence the name). The algorithm scans the list of turning points and, using a short look-back window (usually the two preceding turning points), decides whether the newest extremum closes one or more cycles with previous extrema.
- Cycles are extracted as either *full cycles* (when two half-cycles combine) or *half cycles* (residuals at the beginning or end of the record). Full cycles are counted immediately and removed from the stack of retained extrema; half cycles may be left as residuals to be reported as half-cycles at the end (or paired if later extrema close them).
- Each extracted cycle is described by its *range* (peak-to-valley difference) and its *mean* (average of the two extrema). For fatigue damage, one usually works with the cycle *amplitude* $s = \frac{1}{2}$range and mean $m$.

Rainflow approximates the rainflow/rain-drop splitting of a waveform into cycles: when a peak is large enough relative to preceding ones it will pair with a valley that is far enough behind it. The local rule (compare two most recent absolute ranges and decide) provides a consistent pairing that (i) respects chronological order, (ii) prevents overlapping cycles, and (iii) produces the same cycle set as more elaborate graphical implementations used in the original work. The algorithm runs in linear time in the number of turning-points, with a small constant memory (stack of recent extrema).

The rainflow algorithm thus outputs a sequence of stress amplitudes associated with a number of cycles occuring at this amplitude. When put in a histogram, it gives the cycle-amplitude distribution (as displayed on Figure 2). The frequency domain methods are aimed at estimating this distribution with statistical laws.

# 4 Material Characterization Models

Materials characterization (MC), is a systematic measurement of a material's physical properties, chemical composition, and microstructure. In the context of fatigue analysis, the structural resilience of the material is studied. The S-N curve (also called a Whöler curve or stress-life curve) is a fundamental tool in fatigue analysis that describes the relationship between the cyclic stress amplitude ($S$) applied to a material and the number of cycles until failure occurs ($N_f$) [31]. Figure 3 illustrates a S-N curve. Named after the pioneering work of August Whöler in the 19th century, S-N curves characterize the fatigue strength of materials and form the basis for predicting structural durability under cyclic loading.

Some literature dealing with S-N curve models has been available since Weibull [32] discussed S-N curve models. Schutz [33] discussed the Basquin model [34] within the context of fatigue history for a period of 1838–1996. Kohout and Vechet [35] reviewed a few S-N curve models in relation to a newly proposed model. Bolotin [36] proposed a review of fatigue mechanics spanning crack growth, fatigue, and material characterization models.

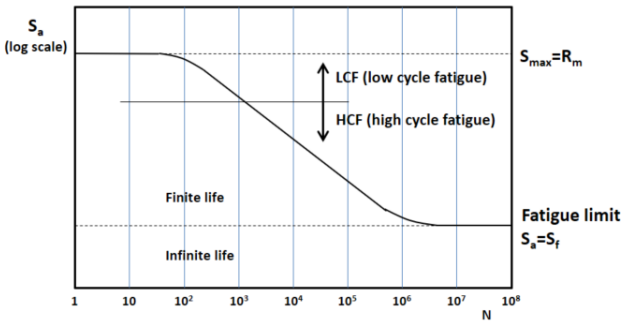


Figure 3: Description of a S-N curve. High-cycle and Low-cycle zones are shown. High-cycle regime corresponds to stress being applied for a large number of cycles. Whereas Low-cycle regime is when stress is being applied a smaller number of cycles. Some MC models are more appropriate for one or the other (or both) depending on the application.

Some S-N curve models were overviewed by Nijssen [37]. Recently, Xiong and Shenoi [38] listed four S-N curve models including Basquin model as the generally accepted ones in a monograph. Buhran [39] proposed the latest review of S-N curves for composite materials giving a critical review of the models cited above. The proposed models in the cited literature can be classified into two groups depending on the approach considered (see Table 1 for consulting the formulas of each model):

- Deterministic models, such as the linear (see Basquin [34]), bilinear (Palmgren [1], Stromeyer [40], Speindel and Haibach [41]) and trilinear rules of sigmoidal curves (Stussi [42], Weibull [32], Kohout and Vechet [35]), among others.
- Probabilistic models, such as Bastenaire [43], Castillo and Canteli [44], and Pascual and Meeker [45], among others

## 4.1 Regimes of Application

Another distinction between each of these models is the regime they apply to. A regime is whether the model accounts for plastic deformation or not. There are two regimes:

- HCF (High Cycle Fatigue), where deformations are elastic, stress is considered to be proportional to strain. In this case S-N models are used.
- LCF (Low Cycle Fatigue), where deformations involve significant plasticity. In this case, Strain-Life ($\varepsilon - N$) models are required.

### 4.1.1 LCF and Dual Models

In Table 1 only one of the presented models is truly designed for the LCF (primarily, but also HCF) regime where plasticity dominates: Coffin-Manson [46, 47]. The equation displays a strain-life relation by summing two components: $\frac{\sigma_f'}{E}(2N_f)^b$ which is the elastic strain component (dominant in HCF), and $\epsilon_f'(2N_f)^c$ which is the plastic strain component (dominant in LCF). Because this model accounts for plastic strain, it is the standard for regimes with high loads and short lives.

The Kohout-Vechet model is another dual-regime model. While technically a Stress-Based model (and thus best for HCF), the authors derived this function to mathematically fit the entire shape of the S-N curve, from the low-cycle "plateau" (ultimate strength region) down to the fatigue limit. It is often cited as a "full-range" S-N model, but it still lacks the explicit plasticity term found in Coffin-Manson.

### 4.1.2 HCF Models

The Basquin model is the simplest power-law description of the S-N curve. It is a straight line in log-log coordinated and does not account for an endurance limit or plasticity. The Stromeyer model is a modification

of the Basquin model that introduces an endurance limit ($S_0$). It models the curve flattening out at high cycles, characterizing infinite life.

The Palmgren model is an early modification to the S-N curve shape to fit experimental data better than a simple power law, specifically near the "knee" of the curve, occuring in high cycle ranges. Similarly, the Speindel-Haibach model is a standardized parametrization of the S-N curve often used in the automotive industry to handle the "knee" point and the variable slope in the high-cycle region. The Stussi model is a non-linear S-N model designed to fit the entire elastic curve better than the Basquin model, particularly covering the endurance limit. The Weibull models the probability of failure at different stress levels. It is highly useful for reliability in HCF where scatter is significant. Note that the Weibull model refers to a deterministic S-N curve shape, and not to the Weibull lifetime distribution also commonly used in this field.

The Bastenaire model is a statistical S-N model often used to describe the S-N curve with a sigmoidal shape, capturing the transition from finite life to the endurance limit. The Castillo-Canteli model is a thermodynamic and statistical based model for the S-N field. It is very adequate for analyzing data scatter in the HCF regime. Finally, the Pascual-Meeker model is a "Random Fatigue Limit" model. It treats the endurance limit ($S_0$) not as a fixed constant but as a random variable, which is critical for probabilistic HCF analysis.

Table 1: Proposed deterministic and probabilistic models in literature for the S–N curves (see Muniz et al. [18] and Castillo [44]).

| **Model** | **Expression** | **Regime** | **Type** |
|---|---|---|---|
| Basquin [34] | $\log N = A - B \log S$ | HCF | Deterministic |
| Coffin-Manson [46, 47] | $\frac{\sigma'_f}{E}(2N_f)^b + \epsilon'_f(2N_f)^c$ | LCF & HCF | Deterministic |
| Stromeyer [40] | $\log N = A - B \log(S - S_0)$ | HCF | Deterministic |
| Palmgren [1] | $\log(N + D) = A - B \log(S - S_0)$ | HCF | Deterministic |
| Weibull [32] | $\log(N + D) = A - B \log\left(\frac{S-S_0}{S_{st}-S_0}\right)$ | HCF | Deterministic |
| Stüssi [42] | $\log N = A - B \log\left(\frac{(S-S_0)}{(S_{st}-S)}\right)$ | HCF | Deterministic |
| Bastenaires [43] | $\big(\log N - B\big)(S - S_0) = A \exp[-C(S - S_0)]$ | HCF | Probabilistic |
| Speindel–Haibach [41] | $\log\left(\frac{N}{N_0}\right) = A \log\left(\frac{S}{S_0}\right) - B \log\left(\frac{S}{S_0}\right) + B \left\{ \frac{1}{\alpha} \log\left[1 + \left(\frac{S}{S_0}\right)^{-2\alpha}\right]\right\}$ | HCF | Deterministic |
| Castillo–Canteli [44] | $\log(N/N_0) = \frac{\lambda + \delta\big(-\log(1-p)\big)^\beta}{\log(S/S_0)}$ | HCF | Probabilistic |
| Kohout–Vechet [35] | $\log\left(\frac{S}{S_\infty}\right) = \log\left(\frac{N+N_1}{N+N_2}\right)^b$ | HCF & LCF | Deterministic |
| Pascual–Meeker [45] | $\log N = A - B \log(S - S_0)$ | HCF | Probabilistic |

The simplest and most widely used models is the Basquin equation [34], which linearizes the high-cycle-fatigue (HCF) regime in a log-log coordinates:

$$N_f.S_a^b = C \text{ or } S_a = (\frac{C}{N_f})^{1/b} \tag{1}$$

where $S_a$ is the stress amplitude, $N_f$ is the number of cycles to failure, and $C$ and $b$ are material constants. Basquin's law is the workhorse for metallic components in the long-life regime and is the default S-N model in most vibration-fatigue software [4, 17].

As mentionned earlier, for low-cycle fatigue (LCF) and cases where plastic strain dominates, the Coffin-Manson relation, introduced in 1954 by Coffin [46] and Manson in 1953 [47], is employed:

$$\frac{\delta\epsilon_p}{2} = \epsilon'_f(2N_f)^c \tag{2}$$

where $\delta\epsilon_p$ is the plastic strain range, $\epsilon'_f$ is the fatigue ductility coefficient, and $c$ is the fatigue ductility exponent. When both elastic and plastic strains are significant , the two contributions are combined into the Manson-Coffin-Basquin (MCB) strain-life equation [48]:

$$\frac{\delta\epsilon}{2} = \frac{\delta\epsilon_e}{2} + \frac{\delta\epsilon_p}{2} = \frac{\sigma'_f}{E}(2N_f)^b + \epsilon'_f(2N_f)^c \tag{3}$$

where $\sigma'_f$ and $b$ are the fatigue strength coefficient and exponent, respectively, and $E$ is the elastic modulus. This unified formulation is essential for vibration problems that span both HCF and LCF, such as in automotive suspension components or wind-turbine gearboxes [49, 50].

Zorman et al. (2023) [12] note that the parameters $C$ and $b$ (or equivalently in Equation 3 $\sigma'_f, b, \epsilon'_f, c$) are treated as deterministic material properties in most TDFA implementations, but they can also be modeled as random variables to account for scatter. Meeker et al. (2022) [49] provide a modern statistical treatment of S-N curves, emphasizing that "the Basquin equation is the simplest, most widely used, and safely conservative model for fatigue life estimation".

The wide panel of available material-characterization models—and the way new formulations have emerged over time—reflects the increasing maturity of the field and its effort to account for real operating conditions that early models could not fully capture. Classical models provide a robust and often conservative baseline, but modern engineering problems frequently demand more specialized approaches. In applications where variability, complexity, or nonlinear behavior play a significant role, probabilistic formulations or enhanced multi-parameter models become more suitable. However, their specificity also limits their general adoption, as they tend to be tailored to particular materials or loading scenarios. In contrast, the foundational models remain widely used because they are straightforward, practically effective, and offer the essential level of fidelity without unnecessary complexity.

# 5 Damage Accumulation Rules

## 5.1 The Palmgren-Miner Linear Damage Accumulation Rule

The life expectancies of parts subjected to spectrum loading are commonly estimated from the empirical Palmgren-Miner damage law, introduced first by Palmgren [1] in the analysis of ball bearings and adapted by Miner [2] for aircraft structures.

Let $n_i$ denote the number of stress cycles with a constant stress amplitude $S_i$ and $N_f$ is the number of cycles with the same amplitude to a specified extent of the damage $\xi$ after which the component is considered to have failed. Miner [2] suggested that in a fatigue test at a constant stress amplitude $S_i$ damage could be regarded to accumulate linearly with the number of cycles. Accordingly, if at a stress amplitude $S_1$ the component has a life of $N_{1f}$ cycles, which corresponds to the amount of damage $\xi$, after $n_1$ cycles at the same stress amplitude, the amount of damage will be $\frac{n_1}{N_{1f}}\xi$. After $n_2$ stress cycles at the same stress amplitude $S_2$, characterized by a fatigue life of $N_{2f}$ cycles, the amount of damage will be $\frac{n_2}{N_{2f}}\xi$ etc. [51]. Failure occurs when, at a certain stress amplitude $S_m$, the sum of the partial amounts of damage attains the amount $\xi$, i.e. when

$$\frac{n_1}{N_{1f}}\xi + \frac{n_2}{N_{2f}}\xi + \cdots + \frac{n_m}{N_{mf}}\xi = \xi \tag{4}$$

is fulfilled. As a result, the analytical expression of the Palmgren-Miner rule becomes

$$\xi = \sum_{i=1}^{M} \frac{n_i}{N_i f} \tag{5}$$

$$D = \sum_{i=1}^{M} \frac{n_i}{N_i f}$$

where $N_{if}$ is the number of cycles to attain the specified amount of damage $\xi$ at a constant stress amplitude $S_i$. Essentially, equation 5 is an additivity rule according to which the total number of stress cycles required to attain a specified level of damage $\xi$ is obtained by adding the absolute durations $n_i$ spent at each stress amplitude $S_i$, until the sum of the relative durations $\frac{n_i}{N_{if}}$ becomes unity. The fraction of expended fatigue life at a particular stress amplitude is the ratio of the number of stress cycles spent at this stress amplitude and the total number of stress cycles of the same stress amplitude needed to attain the specified level of damage (from zero initial damage). It is also assumed that the sequence in which the various stress amplitudes are imposed does not affect the fatigue life [51]. Subsequently we will refer to the accumulated damage as $D$. Practically, if $D$ exceeds or is equal to unity, the material has entered a state of failure. Conversely, any value below unity will represent the amount of life (as a percentage) consumed by the cycles.

**Supporting Example** Take the distribution of cycles and amplitude displayed in Figure 2. Suppose that there is an associated S-N curve to this distribution telling us for each amplitude $S_i$ the number of cycles to failure $N_{f,i}$. That is, at constant amplitude $S_i$, how many cycles can my material endure before breaking (e.g. for amplitude 5 Mpa, my material can withstand 20 cycles, $N_{f,i} = 20$). Now consider the Palmgren-Miner model defined in Equation 5. For each $i$, that is, each different amplitude we have in our cycle-amplitude distribution $(5, 10, 15, 22.5, 25, 27.5$ MPa) we can compute the fraction of the number of cycles $n_i$ (1, 2, 0.5, 0.5, 0.5, 0.5) over their respective number of cycles to failue $N_f$. This gives us the contributing damage of each of these amplitudes. If the sum of all these fractions exceeds 1, then our material enters a state of failure (it breaks). Note that these methods are only used over a very large number of cycles to ensure statistical convergence, this example only illustrates the principles but wouldn't be exploitable.

### 5.1.1 Limitations and Alternatives

Despite its widespread use and simplicity, extensive experimental testing has revealed several significant deficiencies of the Palmgren-Miner rule:

- Experimental data shows that the order of loading matters, contrary to the rule's assumptions. Specifically, the High-Low loading and the Low-High loading phenomena. For the first one, when high-stress cycles are applied first, following by low-stress cycles, the rule is non-conservative (predicts failure too late) [52]. Conversely, when low-stress cycles precede high-stress cycles the rule is conservative (predicts failure too early). In this context, this is known as the linearity assumption error.
- High-stress overloads in a loading sequence can cause crack retardation due to residual stress effects (stress redistribution near the crack tip), actually reducing damage accumulation. Conversely, underloads can accelerate crack growth. The Palmgren-Miner rule cannot capture these nonlinear interactions [53, 54].
- For materials with a fatigue limit (e.g., steels), cycles below the endurance limit should theoretically cause no damage. However, some experimental evidence suggests that such subcritical cycles may have cumulative harmful effects when combined with higher-stress cycles. The Palmgren-Miner rule treats these as harmless (contributing zero damage), potentially missing subtle effects [53].

In practice, most TDFA implementations stick with the linear rule for simplicity, but researchers often compare Miner-derived lives with nonlinear alternatives to quantify the error introduced by the linearity assumption.

## 5.2 Classical Nonlinear and Interaction-Aware Models

### 5.2.1 Nonlinear Cumulative Damage Models

One of the most popular alternatives of the Palmgren-Miner model to tackle the linearity assumption is the Manson-Halford model [55], based on the concept of a nonlinear "damage curve" that shows how damage accumulates nonlinearly with cycle ratio:

$$D(A) = \sum_i (\frac{n_i}{N_i})_i^q, q_i = BN_i^\mu \tag{6}$$

where $q_i$ is a material-dependent exponent that captures nonlinearity, and $B$, $\mu$ are material parameters. This model recognizes that damage accumulation is not linear but follows and accelerating curve, with damage increasing faster as the component approaches failure.

A more recent approach was proposed by Li and Liu (2021) [56] that explicitely incorporates load-sequence effect through a damage-curve exponent that varies with the stress-level transition. The core equation is:

$$D = \sum_{i=1}^{k} (\frac{n_i}{N_{f,i}})^{\Xi_i} \ , \ \Xi_i = a.(\frac{\sigma_i}{\sigma_{i-1}})^b \tag{7}$$

where $\Xi_i$ is the sequence-dependent exponent, $a, b$ are material constants fotted from two-level block tests, and $\sigma_{i-1}$ is the stress amplitude of the preceding block.

The incentive behind this model is that when the load increases (low-high sequence), $\Xi_i > 1$, making the damage contribution from the higher level more sever than Miner would predict – this reflects overload-induced crack acceleration. Conversely, for a high-low sequence, $\Xi_i < 1$, the model captures the essential physics of crack-growth interaction without full fracture mechanics simulation. The authors validated the model against variable amplitude vibration tests on steel bridges, showing that it reduces prediction error from $\approx 30\%$ (Miner) to within 10%.

### 5.2.2 Fatigue-Modulus-Based Damage Models

Hwang and Han (1986) [57] introduced three alternative cumulative damage models derived from the degradation of the fatigue modulus $F(n)$, defined as the slope of the stress-strain hysteresis loop at cycle $c$. Their work is particularly valuable for composite materials, where stiffness degradation is a measurable surrogate for internal damage. The models are formulated in terms of a damage variable $D$ that evolves with the resultant strain $\epsilon$ and the normalized cycle ration $n/N_f$:

- Model I (strain-based)
$$D = \frac{\epsilon(n) - \epsilon_0}{\epsilon_f - \epsilon_0} = (\frac{n}{N_f})^\alpha$$
where $\epsilon_0$ is the initial strain, $\epsilon_f$ the strain at failure, and $\alpha$ a material constant.

- Model II (Modulus-based)
$$D = \frac{F(0) - F(n)}{F_0 - F(N_f)} = (\frac{n}{N_f})^\beta$$
with $\beta$ controlling the curvature of modulus decay.

- Model III (Hybrid)
$$D = \frac{\sigma_{max} - \sigma(n)}{\sigma_{max} - \sigma_f} = (\frac{n}{N_f})^\gamma$$
liking residual strength $\sigma(n)$ to the cycle ratio.

Hwang and Han argued that macroscopic stiffness loss directly reflects the accumulation of micro-cracks, fiber breakage, or matrix debonding. The exponents $\alpha, \beta, \gamma$ quantify how rapidly the damage accelerates toward failure; they are not constant but depend on stress level, introducing a load-level dependence that the linear

rule lacks. For metallic structures, similar ideas translate into residual-strength or residual-stiffness models, where the damage rate is tied to the fraction of life consumed at each stress amplitude [57, 58].

### 5.2.3 A Taxonomy of Cumulative Damage Theories

Fatemi and Yang (1998) [59, 60] provided a comprehensive review and classification of cumulative damage models into six categories, each with distinct physical motivations and mathematical structures:

- Linear damage rules - Palmgren-Miner and its variants (e.g. modified Miner with critical damage different than unity).
- Nonlinear damage-curve and two-stage linearization - e.g. Manson's Double Linear Damage Rule [61], which splits life into crack-initiation and crack-propagation phases.
- Life-curve modification methods - Adjust the S-N curve based on prior damage (e.g. the Damaged Stress Model [62]).
- Crack-growth-based approaches - Integrate Paris-law [63] type crack growth over variable-amplitude loading.
- Continuum-damage mechanics (CDM) models - Define a damage variable $D$ that evolves according to a differential equation $\frac{dD}{dn} = f(\sigma, D)$.
- Energy-based theories - Accumulate plastic strain energy or hysteresis per cycle.

The mathematical equation they propose for comparing models is:

$$D = \sum_{i=1}^{k} \int_{0}^{n_i} \frac{dD}{dn}|_{\sigma_i, D} dn \text{ with } D_{cr} = 1 \tag{8}$$

This integral form emphasizes that the damage rate may depend on the current damage state (nonlinear) and on the instantaneous stress $\sigma_i$. Fatemi and Yang stress that load-sequence effects arise naturally when $dD/dn$ is not separable, i.e. when the damage increment at cycle $n$ depends on the history of $D$.

### 5.2.4 Damaged Stress Model (DSM)

Zengah, Aid and Benguediab (2011) [64] revisited the 2005 version of the Damages Model specifically for random vibration fatigue where the load history is reconstructed after rainflow counting. The DSM defines and equivalent stress that accounts for the damage inherited from the previous cycles:

$$\sigma_{eq}^{(i+1)} = \sigma_{i+1}.\Phi(D_i) \ , \ \Phi(D_i) = \frac{1}{1 - D_i} \tag{9}$$

and the damage increment is:

$$\delta D_i = \frac{1}{N_f(\sigma^(i)_{eq}} \tag{10}$$

One could interpret this model as such: as damage accumulates, the material's effective load-bearing cross-section is reduced, so the same nominal stress $\sigma_{i+1}$ produces a higher local stress. The factor $\Phi(D_i)$ amplifies the stress for subsequent cycles, creating a positive feedback that accelerates damage toward the end of life – this captures the "creep-like" acceleration observed experimentally. The model is particularly suited to high-cycle random vibration because it works cycle-by-cycle with rainflow extracted cycles and requires no additional material parameters beyond those requires by the S-N curve [65].

### 5.2.5 Probabilistic Miner's Rule and Deterministic Equivalent Damage

Cartiaux (2024) [66] developed a probabilistic formalization of Miner's rule that bridges deterministic fatigue analysis with structural reliability theory. They introduce a random health variable $H$ for each material volume:

$$H(t) = 1 - \int_0^t \frac{dn}{N_f(\sigma(n))} \tag{11}$$

Failure occurs when $H \leq 0$. The survival probability of a structure under random loading is:

$$P_s(T) = exp(-\int_V \lambda(x)dV) \ , \ \lambda(x) = (\frac{D_{eq}(x)}{D_{cr}})^m \tag{12}$$

where $D_{eq}$ is the deterministic equivalent damage:

$$D_{eq} = \mathbb{E}[\sum_{i=1}^{N_{cycles}} \frac{1}{N_f(\sigma_i}] \tag{13}$$

and $m$ is the Weibull shape parameter from the S-n scatter band.

The classical Miner sum in reinterpreted as the mean damage rate of a random process; the actual damage in a given specimen follows a distribution. The weakest-link principle leads to an overestimation of life because it assumes independence of elementary volumes, ignoring that high-damage zones accelerate neighboring damage. The authors show that the determinstc equivalent damage concept captures the variability of loading severity (e.g. from vibration PSD) without Monte-Carlo simulation, while the probabilistic framework corrects the systematic bias of deterministic Miner. Their case study on an industrial steel beam demonstrates that the conventional approach overstimates life by a factor $> 2$, whereas the probabilistic model aligns with experimental survival curves [67].

Each model builds on its predecessors: Hwang and Han [57] introduced load-level dependence, Fatemi and Yang [59] systematized nonlinear mechanisms, Zengah [64] added stress amplification, Li and Liu [56] incorporated explicit sequence effects, and Cartiaux [66] provided a probabilistic rigor that resolves the long-standing overestimation bias of deterministic Miner's rule. Together, they form a comprehensive toolkit for time-domain vibration fatigue that ranges from the simplest linear summation to full stochastic reliability analysis. Table 2 proposes a comparison between each of the introduced models.

# 6 Application and Comparison with Frequency-Domain Methods

Because TDFA is computationally expensive, the development of frequency-domain methods that estimate damage directly from the Power Spectral Density (PSD) of the stress process has increased. Every major spectral method is validated by comparing its predicted damage to TDFA damage computed on Monte-Carlo-generated stress histories [68, 69].

Zorman et al. (2023) state explicitly: "The accuracy of the spectral methods is investigated in terms of a time-domain rainflow analysis, where three different materials are considered: steel, aluminium and spring steel". Their open-source Python package FLife uses rainflow + Miner as the reference and reports relative error for each spectral estimator [12].

Slavič et al. (2013) [4] performed an extensive experimental validation: "The fatigue-life estimates for the frequency-domain methods were compared to the life estimate in the time domain using a combination of the rainflow count and the Palmgren-Miner hypothesis, TRFC, which in this study is assumed to be an exact reference value". They found that the Zhao-Baker [70] method was most accurate and conservative for automotive vibration profiles, while Dirlik [71] and Tovo-Benasciutti [72] performed nearly as well.

Halfpenny (1999) [17] reaches a similar conclusion: "The Dirlik formulation... has been found to be widely applicable and constantly outperforms all of the other available methods" when benchmarked against rainflow + Miner on wide-band marine spectra. He attributes Dirlik's success to its empirical fit to rainflow-range distributions derived from thousands of simulated time histories.

Thus, the literature uniformly treats time-domain rainflow + Miner as the ground truth. Spectral methods are judged by how closely they replicate TDFA results while offering orders-of-magnitude speed improvements. This

| Model | Mathematical Form | Key Physical Idea | Vibration-Fatigue Relevance |
|---|---|---|---|
| Palmgren–Miner [1, 2] | $D = \sum n_i/N_{f,i}$ | Linear, history-independent | Baseline for time-domain rainflow |
| Manson–Halford [47] | $D = BN_i^{\mu}$ | Nonlinear, history aware, material dependent | Captures nonlinear relations between damage and cycle ratio |
| Hwang & Han (Modulus) [57] | $D = (n/N_f)^{\alpha,\beta,\gamma}$ | Stiffness/strength degradation | Captures load-level dependence |
| Fatemi & Yang Taxonomy [59] | $\frac{dD}{dn} = f(\sigma, D)$ | Six categories, unified framework | Guides model selection |
| Damaged Stress Model [64] | $\sigma_{eq} = \frac{\sigma}{1-D}$ | Stress amplification by damage | Cycle-by-cycle random loading |
| Li & Liu (Sequence) [56] | $D = \sum (n_i/N_{f,i})^{\xi_i}$ | Load-sequence exponent | Vibration overload/retardation |
| Cartiaux (Probabilistic) [66] | $P_s = \exp\left(-\int \lambda \, dV\right)$ | Random health, equivalent damage | Structural reliability, PSD loading |

Table 2: Comparison of representative fatigue damage accumulation models and their relevance to vibration-fatigue analysis.

validation paradigm is the central theme of the four key references and is repeated across dozens of comparative studies.

Across most engineering domains, modern fatigue-assessment practice increasingly relies on frequency-domain methods rather than full time-domain simulation. This shift is driven by two main factors: the prevalence of broadband or narrow-band vibration environments and the substantial computational savings offered by spectral techniques as mentioned several times. Methods such as Dirlik, Zhao–Baker, or Tovo–Benasciutti can extract damage rates directly from stress or acceleration PSDs without generating long stress time histories, making them well-suited for early-stage design, optimization loops, and system-level trade studies [68]. Their efficiency is especially valuable for large structures (airframes, offshore jackets) or components subjected to long-duration stochastic loading (automotive suspensions, wind-turbine blades) [4]. However, frequency-domain approaches rely on assumptions—Gaussianity, stationarity, linearity—that are not always satisfied in real loading conditions. For this reason, time-domain rainflow counting remains the reference method for final verification, particularly when dealing with nonlinearities, overload events, transient conditions, or multi-axial interactions [12]. In contemporary workflows, spectral methods provide the primary life estimates, while time-domain analyses serve as the high-fidelity check that ensures regulatory compliance and captures damage mechanisms that frequency-domain formulations may under-predict.

# 7 Fatigue Damage Spectrum and Maximum Response Spectrum

The Fatigue Damage Spectrum (FDS) and the Maximum/Extreme Response Spectrum (MRS/ERS), mostly presented by Christian Lalanne [73], are widely used damage indicators for quantifying the severity of vibration environments. Although typically evaluated in the frequency domain, both metrics originate from time-domain excitation and quantify its effect by computing the accumulated fatigue damage or extreme response of hypothetical single-degree-of-freedom (SDOF) oscillators over a range of natural frequencies. By reducing complex, non-stationary vibration signals to equivalent damage or peak response measures, FDS and MRS/ERS provide a physically meaningful link between time-domain loading and structural response. As a result, they have become cornerstone tools in vibration test tailoring, enabling the development of accelerated laboratory tests that reproduce the fatigue damage and peak stresses encountered by components under real operational conditions [74].

## 7.1 Theoretical Foundations

Both spectra rest on an assumption originally proposed by Biot in 1932 [75] for earthquakes analysis: that an unkown structural component can be modelled as an SDOF oscillator with some natural frequency and damping ratio. The Shock Response Spectrum (SRS), which predates MRS/ERS, plots the maximum displacement response of such an SDOF system against its natural frequency for a given transient input. In 1981, D.O Smallwood [76] introduced a recursive formula for calculating shock response spectra called the Z-transform directly from the time signal. Lalanne extended this concept to random vibration and fatigue by introducing closed-form expressions for both the expected maximum response (ERS/MRS) and cumulative fatigue damage (FDS) directly from the input power spectral density (PSD) [77].

## 7.2 Continuous SDOF base-excited model

The response of SDOF oscillators to a measured time signal is most often computed using discrete-time recursive filters from the continuous SDOF equation, with D.O. Smallwood's [76] Z-transform-based "ramp invariant" filter now the standard approach.

For a base-excited SDOF system (mass $m$, damping $c$, stiffness $k$) subjected to a measured based acceleration $\ddot{x}_s(t)$, the relative displacement $z(t) = x(t) - x_s(t)$ satisfies:

$$m\ddot{z}(t) + c\dot{z}(t) + kz(t) = -m\ddot{x}_s(t) \tag{14}$$

with natural circular frequency $\omega_n = \sqrt{k/m}$ and damping ratio $\xi = c/(2m\omega_n)$. In MRS/FDS work, this equation is solved for many oscillations $\omega_n, \xi$ using the same measured input $\ddot{x}_s(t)$; the MRS uses the maximum of the SDOF response in relative displacement, and the FDS uses the response history for fatigue analysis [78].

### 7.2.1 Discrete-time formulation and Z-transform

Let the measured base acceleration be sampled at interval $\Delta t$, giving the time sequence $\ddot{x}_s[k] = \ddot{x}_s(k\Delta t)$. For each SDOF, one seeks a recursion of the form [76]:

$$z[k] = a_1 z[k-1] + a_2 z[k-2] + b_0\ddot{x}_s[k] + b_1\ddot{x}_s[k-1] + b_2\ddot{x}_s[k-2] \tag{15}$$

or more generally, for response quantity $y[k]$:

$$y[k] = -\alpha_1 y[k-1] - \alpha_2 y[k-2] + \beta_0\ddot{x}_s[k] + \beta_1\ddot{x}_s[k-1] + \beta_2\ddot{x}_s[k-2] \tag{16}$$

with parameters $\alpha_i$ and $\beta_j$:

- $\beta_0 = \frac{1}{\omega_0 dt}[2(C-1) + \frac{2\xi^2-1}{\sqrt{1-\xi^2}}S] + \omega_0 dt$
- $\beta_1 = \frac{1}{\omega_0 dt}[-2C\omega_0 dt + 2\xi(1-E)^2 - 2\frac{2\xi^2-1}{\sqrt{1-\xi^2}}S]$

- $\beta_2 = \frac{1}{\omega_0 dt}[E^2(\omega_0 dt + 2\xi) - 2\xi C + \frac{2\xi^2 - 1}{\sqrt{1-\xi^2}} S]$
- $\alpha_1 = -2C$
- $\alpha_2 = E^2$

and parameters $E$, $C$, and $S$ being:

- $E = e^{-\xi\omega_0 dt}$
- $C = Ecos(\omega_d dt)$
- $S = Esin(\omega_d dt)$
- $\omega_0 = 2\pi f_n$
- $\omega_d = \omega_0\sqrt{1-\xi^2}$

with $f_0$ being the frequency of the studied SDOF resonator.

Taking the Z-transform of the continuous transfer function and requiring that the discrete response matches the continuous response under specific basis functions (impulse or ramp) leads to the coefficients $\alpha_i$ and $\beta_j$.

Two variants exist of this method. The first one, the impulse-invariant method, matches the continuous impluse response at discrete time instants; convenient but introduces errors in DC and low-frequency behaviour for base-excited problems [79]. The second one, the ramp-invariant method proposed by Smallwood as an improvement, assumes the the input is piecewise linear between samples and matches the continuous response to a unit-slope ramp over each interval; it preserves the correct low-frequency response and reduces aliasing. The Smallwood's improved recursive formula is ramp-invariant and is generally preferred for MRS and FDS computations where correct low-frequency response is critical.

## 7.3 Maximum Response Spectrum

Miles (1954) [80] showed that the RMS displacement response of a lightly-damped SDOF oscillator to a white-noise base acceleration can be written as a simple function of the PSD level at the natural frequency, damping, and natural frequency itself. Lalanne (1978) [73] refined this by recognising that the peaks of a narrow-band response follow a Rayleigh distribution rather than a Gaussian one, and derived the expected extreme response over a given duration $T$:

$$MRS(f_n) = \sqrt{\pi Q f_n G_{\ddot{z}}(f_n) \ln(f_n T)} \tag{17}$$

where $Q$ is the dynamic amplification factor, $G_{\ddot{z}}$ is the input acceleration PSD at frequency $f_n$, and logarithmic term accounts for the statistics of extremes over the observation time. The MRS therefore indicates the most likely peak response a component would experience if it had a resonance at each frequency, making it useful for clearance checks and yield-limit verification [81].

## 7.4 Fatigue Damage Spectrum

Building on work by Bendat [82] and Rice [83] on spectral fatigue, Lalanne [84] proposed a closed-form expression for the fatigue damage accumulated by an SDOF oscillator excited by a random PSD:

$$FDS(f_n) = T f_n K^b (\pi Q f_n G_{\ddot{z}}(f_n))^{\frac{b}{2}} \frac{\Gamma(1 + \frac{b}{2})}{C} \tag{18}$$

where $b$ and $C$ are material S-N curve parameters (remember the Basquin Law $N = CS^{-b}$), $\Gamma(.)$ is the Gamma function, and $K$ relates displacement to stress. The FDS thus indicates, for each hypothetical resonance frequency, how much fatigue damage a component would accumulate over the test duration, assuming Palmgren-Miner linear damage accumulation [81].

## 7.5 Physical Interpretation

On one hand, the MRS answers the question: *"If my structure has a single dominant mode at frequency $f_n$, what is the largest instantaneous stress it would likely see during this vibration ?"*. It is analogous to the SRS for transient shocks but applied to stationary random vibration of arbitrary duration. A higher MRS at a given frequency greater risk of exceeding yield of clearance limits for components resonating near that frequency.

On the other hand, the FDS answers a different question: *"How damaging is this vibration to a component whose fatigue life is dominated by a mode at frequency $f_n$ ?"*. Because fatigue damage accumulates over millions of low-amplitude cycles, the FDS integrates the effect of the entire stress-cycle distribution, weighted by the S-N curve exponent. A higher FDS at a frequency means that components with resonance there will accumulate more fatigue damage.

Both MRS and FDS are complementary: the MRS protects against instantaneous overload while the FDS protects against long-term fatigue. In test tailoring, engineers ensure that the synthesised test PSD has an MRS below the SRS (to avoid unrealistic peak loads) while its FDS matches or exceeds the cumulative field FDS (to guarantee equivalent fatigue damage).

## 7.6 Construction Methods

For the MRS, Equation 16 is used to compute the response $y[k]$ for each SDOF oscillator over the entire time record and each frequencies $f_n$ being studied [77]:

- For each $f_n$ compute $\omega_0, \omega_d, E, C, S$ and the coefficients $\alpha_1, \alpha_2, \beta_0, \beta_1, \beta_2$.
- Filter the base acceleration time sequence $\ddot{x_s}[k]$ to obtain the response sequence $y[k]$.
- The MRS ordinate at that frequency is a formula using the maximum of the response at given frequency $\max_k |y[k]|$.

An example of formula used to build the MRS unit indicator at frequency $f_0$ is:

$$MRS(f_0) = (2\pi f_0)^2 \max_k |y[k]| \tag{19}$$

involving the frequency, a circular motion illustrated by the factor $\pi$ and the maximum of the response of the SDOF resonator.

For the FDS, again, Equation 16 is used to compute the response $y[k]$ for each SDOF oscillator over the entire time record and each frequencies $f_n$ being studied [77]:

- For each $f_n$, $\omega_0, \omega_d, E, C, S$ and the coefficients $\alpha_1, \alpha_2, \beta_0, \beta_1, \beta_2$.
- Filter the base acceleration time sequence $\ddot{x_s}[k]$ to obtain the response sequence $y[k]$.
- Apply rainflow cycle counting method to obtain a set of stress ranges and counts.
- Use the appropriate S-N curve model and damage accumulation rule to compute damage at that frequency; repeat for each frequency to build the FDS.

An example of S-N curve model and damage accumulation model could be the combination of the Basquin Model and the Palmgren-Miner linear accumulation rule. Thus giving the FDS formula for frequency $f_0$:

$$FDS(f_0) = \frac{K^b}{c} \Sigma_i n_i (z_{i,\xi,f_0})^b \tag{20}$$

with $K, c$, and $b$ being material parameters associated to the S-N model, $n_i$ the number of cycles at frequency $f_0$ for a given response $z$ of resonator with damping coefficient $\xi$ and natural frequency $f_0$.

The physical interpretation is that each digital filter represents a virtual mode of the structure, and the recursion is tracking how that mode accumulates cycles of stress over the recorded environment. The ramp-invariant formulation ensures that low-frequency, quasi-static contributions are correctly represented, which is crucial because fatigue damage is highly sensitive to stress amplitude [76]. In Figure 4, the MRS peak in the center

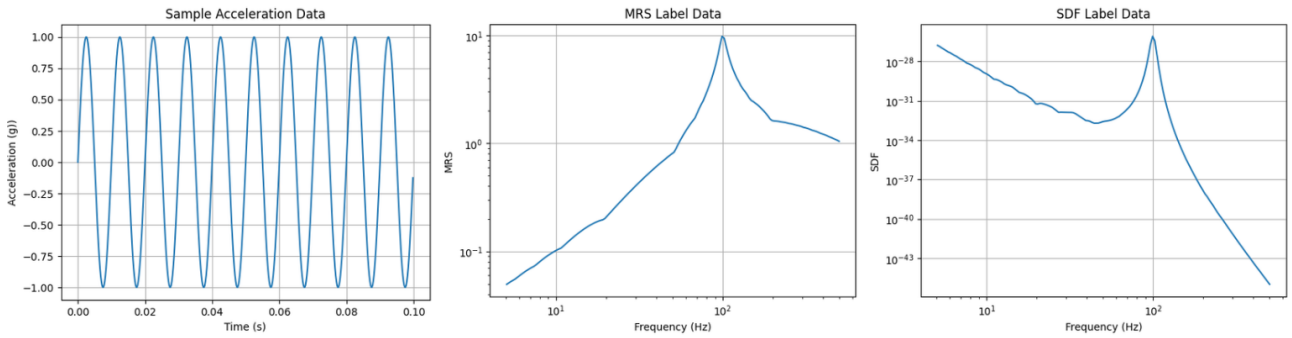


Figure 4: *Left*: Deterministic single-frequency sinusoidal acceleration used as validation input. *Center*: Maximum Response Spectrum (MRS) computed from the SDOF responses, showing a clear resonance peak at the excitation frequency, with an amplitude consistent with the theoretical dynamic amplification factor $Q = 1/(2\zeta)$. *Right*: Fatigue Damage Spectrum (FDS) obtained from rainflow cycle counting and a Miner–Basquin damage model, exhibiting a sharp damage concentration at resonance due to the strong sensitivity of fatigue damage to response amplitude. Results were obtained with our own implementation of the Rainflow algorithm, Z-transform SDOF filter, and MRS/FDS computation.

panel occurs at the excitation frequency, confirming that the SDOF response is correctly amplified at resonance and attenuated away from it, in accordance with linear vibration theory. The FDS in the right panel shows a much sharper frequency localization than the MRS, reflecting the nonlinear dependence of fatigue damage on cycle amplitude through the Basquin exponent. Although both spectra peak at the same frequency, their shapes differ fundamentally: the MRS characterizes extreme dynamic response, whereas the FDS quantifies cumulative fatigue damage driven by cyclic loading.

Alternative time-domain methods for computing SDOF response include [85]:

- Direct numerical integration of the differential equation (e.g. Newmark-$\beta$ or Runge-Kutta)
- Convolution/Duhamel intergral evaluated by numerical quadrature
- FIR filters approximating the impulse response

These methods can be more general but are typically less efficient than the IIR recursion, especially when hundreds of SDOF oscillators are needed for a dense ERS/FDS. Smallwood's ramp-invariant filter is preferred in practice because it combines:

- Exact continuous-time behaviour for linear ramps between samples.
- Good low-frequency accuracy and DC response.
- High numerical efficiency and stability for large number of oscillators.

In the context of Lalanne's framework, this discrete-time approach provides the essential bridge between measured time signals and the response-based spectra (MRS and FDS) used for test tailoring and damage equivalence [78]. This method lies at the intersection of time-domain analysis and frequency-domain results, naturally calling towards methods in the time-frequency domain allowing for frequency component detection as well as their time-variant features.

# References


[1]A. Palmgren, "Die lev/bensdauer von kugellagern", VDI. Z. **68**, 339–341 (1924).

[2]M. A. Miner, "Cumulative damage in fatigue", (1945).

[3]M. Matsuishi and T. Endo, "Fatigue of metals subjected to varying stress", Japan society of mechanical engineers, Fukuoka, Japan **68**, 37–40 (1968).

[4]M. Mršnik et al., "Frequency-domain methods for a vibration-fatigue-life estimation – Application to real data", International Journal of Fatigue **47**, 8–17 (2013).

[5]J. M. Elson and J. M. Bennett, "Calculation of the power spectral density from surface profile data", Applied optics **34**, 201–208 (1995).

[6]K. Hectors and W. De Waele, "Cumulative damage and life prediction models for high-cycle fatigue of metals: a review", Metals **11**, 204 (2021).

[7]Department of Structure and Materials, Faculty of Mechanical Engineering, Universiti Teknikal Malaysia Melaka, Hang Tuah Jaya, 76100 Durian Tunggal, Melaka, MALAYSIA et al., "A Review of the Loading Sequence Effects on the Fatigue Life Behaviour of Metallic Materials", JESTR **9**, 189–200 (2016).

[8]T. Huang et al., "A modified model for nonlinear fatigue damage accumulation of turbine disc considering the load interaction effect", Metals **9**, 919 (2019).

[9]H. Gao et al., "A modified nonlinear damage accumulation model for fatigue life prediction considering load interaction effects", The Scientific World Journal **2014**, 164378 (2014).

[10]S. Gupta and A. Ray, "Real-time fatigue life estimation in mechanical structures", Measurement Science and Technology **18**, 1947 (2007).

[11]Y. Wang et al., "A hybrid frequency-time domain life prediction method based on the critical plane theory", Fatigue & Fracture of Engineering Materials & Structures **47**, 2351–2368 (2024).

[12]A. Zorman et al., "Vibration fatigue by spectral methods—a review with open-source support", Mechanical systems and signal processing **190**, 110149 (2023).

[13]R. R. Craig Jr and A. J. Kurdila, *Fundamentals of structural dynamics* (John Wiley & Sons, 2006).

[14]D. J. Inman, *Engineering vibration*, Fifth edition (Pearson, Hoboken, NJ, 2022).

[15]M. Zóltowski, R. Martinod, et al., "Technical condition assessment of masonry structural components using frequency response function (frf)", Masonry International (2016).

[16]N. Dowling, "Fatigue life prediction for complex load versus time histories", Journal of Engineering Materials and Technology **105**, 206–214 (1983).

[17]A. Halfpenny, "A Frequency Domain Approach for Fatigue Life Estimation from Finite Element Analysis", Key Engineering Materials **167–168**, 401–410 (1999).

[18]M. Muñiz-Calvente et al., "A comparative review of time-and frequency-domain methods for fatigue damage assessment", International Journal of Fatigue **163**, 107069 (2022).

[19]D. Chelidze et al., "Fatigue life estimation of structures under statistically and spectrally similar variable amplitude loading", Mechanical Systems and Signal Processing **161**, 107856 (2021).

[20]S.-C. Tien et al., "Energy-based time derivative damage accumulation model under uniaxial and multiaxial random loadings", Fatigue & Fracture of Engineering Materials & Structures **45**, 159–173 (2022).

[21]L. Zhang et al., "A modified damaged stress model for fatigue life prediction based on load interaction", Heliyon **10** (2024).

[22]B. Ligaj, "An analysis of the influence of cycle counting methods on fatigue life calculations of steel", Scientific problems of machines operation and maintenance **4**, 25–43 (2011).

[23]T. Kebir et al., "Numerical study of fatigue damage under random loading using rainflow cycle counting", International Journal of Structural Integrity **12**, 149–162 (2021).

[24]S. Arıduru, "Fatigue life calculation by rainflow cycle counting method", MA thesis (Middle East Technical University, 2004).

[25]A. K. Khosrovaneh and N. Dowling, "Fatigue loading history reconstruction based on the rainflow technique", International Journal of Fatigue **12**, 99–106 (1990).

[26]D. Socie, "Rainflow cycle counting: a historical perspective", The Rainflow Method in Fatigue, 3–10 (1992).

[27]I. Rychlik, "A new definition of the rainflow cycle counting method", International Journal of Fatigue **9**, 119–121 (1987).

[28]G. Marsh et al., "Review and application of rainflow residue processing techniques for accurate fatigue damage estimation", International Journal of Fatigue **82**, 757–765 (2016).

[29]Y. Ling et al., "Stochastic characterization and update of fatigue loading for mechanical damage prognosis", in Annual conference of the phm society, Vol. 2, 1 (2010).

[30]C. Amzallag et al., "Standardization of the rainflow counting method for fatigue analysis", International journal of fatigue **16**, 287–293 (1994).

[31]C. M. Sonsino, "Course of SN-curves especially in the high-cycle fatigue regime with regard to component design and safety", International Journal of Fatigue **29**, 2246–2258 (2007).

[32]A. J. Hallinan Jr, "A review of the weibull distribution", Journal of quality technology **25**, 85–93 (1993).

[33]W. Schütz, "A history of fatigue", Engineering fracture mechanics **54**, 263–300 (1996).

[34]O. BASQUIN, *The exponential law of endurance tests american society for testing and materials, 1910.*

[35]J. Kohout and S. Ve˘chet, "A new function for fatigue curves characterization and its multiple merits", International Journal of Fatigue **23**, 175–183 (2001).

[36]V. V. Bolotin, *Mechanics of fatigue* (Crc Press, 2020).

[37]R. Nijssen, "Phenomenological fatigue analysis and life modelling, fatigue life prediction of composites and composite structures, ed. by anastasios p", Vassilopoulos, Woodhead Publ. Ltd and CRC Press LLC (2010).

[38]J. J. Xiong and R. A. Shenoi, *Fatigue and Fracture Reliability Engineering* (Springer Science & Business Media, Jan. 2011).

[39]I. Burhan and H. S. Kim, "Sn curve models for composite materials characterisation: an evaluative review", Journal of Composites Science **2**, 38 (2018).

[40]C. Stromeyer, "The determination of fatigue limits under alternating stress conditions", Proceedings of the Royal Society of London. Series A, Containing Papers of a Mathematical and Physical Character **90**, 411–425 (1914).

[41]J. Spindel and E. Haibach, "Shape of s-n curves", Statistical analysis of fatigue data **744**, 89 (1981).

[42]F. Stüssi, *Die theorie des dauerfestigkeit und die versuche von august wöhler* (Verlag VSB, 1955).

[43]F. Bastenaire, *New method for the statistical evaluation of constant stress amplitude fatigue-test results* (ASTM International, 1972).

[44]E. Castillo et al., "Statistical model for fatigue analysis of wires, strands and cables", in Iabse proceedings (1985), pp. 1–40.

[45]F. G. Pascual and W. Q. Meeker, "Estimating fatigue curves with the random fatigue-limit model", Technometrics **41**, 277–289 (1999).

[46]L. F. Coffin Jr, "A study of the effects of cyclic thermal stresses on a ductile metal", Transactions of the American Society of Mechanical engineers **76**, 931–949 (1954).

[47]S. S. Manson, *Behavior of materials under conditions of thermal stress*, Vol. 2933 (National Advisory Committee for Aeronautics, 1953).

[48]S. Schmitz et al., "A probabilistic model for lcf", Computational Materials Science **79**, 584–590 (2013).

[49]W. Q. Meeker et al., "Modern statistical models and methods for estimating fatigue-life and fatigue-strength distributions from experimental data", arXiv preprint arXiv:2212.04550 (2022).

[50]E. Santecchia et al., "A review on fatigue life prediction methods for metals", Advances in Materials Science and Engineering **2016**, 9573524 (2016).

[51]M. T. Todinov, "Necessary and sufficient condition for additivity in the sense of the Palmgren–Miner rule", Computational Materials Science **21**, 101–110 (2001).

[52]K. Hectors and W. De Waele, "Cumulative Damage and Life Prediction Models for High-Cycle Fatigue of Metals: A Review", Metals **11**, 204 (2021).

[53]K. A. Zakaria et al., "A review of the loading sequence effects on the fatigue life behaviour of metallic materials", Journal of Engineering Science and Technology Review **9**, 189–200 (2024).

[54]B.-T. Huang et al., "Fatigue Deformation Model of Plain and Fiber-Reinforced Concrete Based on Weibull Function", Journal of Structural Engineering **145**, 04018234 (2019).

[55]S. S. Manson and G. R. Halford, *Fatigue and durability of metals at high temperatures* (ASM International, 2009).

[56]H. Li et al., "New nonlinear cumulative fatigue damage model based on ecological quality dissipation of materials", International Journal of Aerospace Engineering **2021**, 5555812 (2021).

[57]W. Hwang and K. Han, "Cumulative damage models and multi-stress fatigue life prediction", Journal of composite materials **20**, 125–153 (1986).

[58]W. Hwang and K. S. Han, "Fatigue of composites—fatigue modulus concept and life prediction", Journal of Composite Materials **20**, 154–165 (1986).

[59]A. Fatemi and L. Yang, "Cumulative fatigue damage and life prediction theories: a survey of the state of the art for homogeneous materials", International journal of fatigue **20**, 9–34 (1998).

[60]L. Yang and A. Fatemi, "Cumulative fatigue damage mechanisms and quantifying parameters: a literature review", Journal of testing and evaluation **26**, 89–100 (1998).

[61]S. Manson and G. R. Halford, "Practical implementation of the double linear damage rule and damage curve approach for treating cumulative fatigue damage", International journal of fracture **17**, 169–192 (1981).

[62]G. Mesmacque et al., "Sequential law in multiaxial fatigue, a new damage indicator", International Journal of Fatigue **27**, 461–467 (2005).

[63]N. Pugno et al., "A generalized paris' law for fatigue crack growth", Journal of the Mechanics and Physics of Solids **54**, 1333–1349 (2006).

[64]A. Aıd et al., "Fatigue life prediction under variable loading based on a new damage model", Materials & Design **32**, 183–191 (2011).

[65]S. Zengah et al., "Comparative study of fatigue damage models using different number of classes combined with the rainflow method", Engineering, Technology & Applied Science Research **3**, 446–451 (2013).

[66]F.-B. Cartiaux et al., "Survival probability of structures under fatigue: a data-based approach", Probabilistic Engineering Mechanics **77**, 103657 (2024).

[67]F.-B. Cartiaux et al., "Probabilistic formulation of miner's rule and application to structural fatigue", Probabilistic Engineering Mechanics **74**, 103500 (2023).

[68]T. Dirlik and D. Benasciutti, "Dirlik and Tovo-Benasciutti Spectral Methods in Vibration Fatigue: A Review with a Historical Perspective", Metals **11**, 1333 (2021).

[69]M. Mršnik et al., "Vibration fatigue using modal decomposition", Mechanical Systems and Signal Processing **98**, 548–556 (2018).

[70]W. Zhao and M. J. Baker, "On the probability density function of rainflow stress range for stationary Gaussian processes", International Journal of Fatigue **14**, 121–135 (1992).

[71]T. Dirlik, "Application of computers in fatigue analysis", PhD thesis (University of Warwick, Jan. 1985).

[72]R. Tovo, "Cycle distribution and fatigue damage under broad-band random loading", International Journal of Fatigue **24**, 1137–1147 (2002).

[73]C. Lalanne, "Simulation of mechanical shock environments", (1975).

[74]A. Halfpenny, "Accelerated vibration testing based on fatigue damage spectra", White paper, nCode International, www. ncode. com (2006).

[75]M. A. Biot, "Transient oscillations in elastic systems", PhD thesis (California Institute of Technology, 1932).

[76]D. O. Smallwood et al., "An improved recursive formula for calculating shock response spectra", Shock and vibration bulletin **51**, 211–217 (1981).

[77]C. Lalanne, *Mechanical vibration and shock analysis, fatigue damage*, Vol. 4 (John Wiley & Sons, 2014).

[78]S. I. McNeill, "Implementing the fatigue damage spectrum and fatigue damage equivalent vibration testing", in 79th shock and vibration symposium: october, Vol. 26 (2008), p. 30.

[79]T. Irvine, "Modal transient analysis of a system subjected to an applied force via a ramp invariant digital recursive filtering relationship", Revision K, Vibrationdata (2012).

[80]J. W. MILES, "On Structural Fatigue Under Random Loading", Journal of the Aeronautical Sciences **21**, 753–762 (1954).

[81]D. Cho, "Evaluation of vibration test severity by fds and ers", in Proceedings of isma (2010), pp. 1725–1736.

[82]J. S. Bendat and A. G. Piersol, *Random Data: Analysis and Measurement Procedures* (John Wiley & Sons, Sept. 2011).

[83]S. O. Rice, "Mathematical analysis of random noise", The Bell System Technical Journal **23**, 282–332 (1944).

[84]C. Lalanne, "Fatigue damage spectrum of a random vibration", Specification Development, 125–163 (2014).

[85]J. Liu et al., "Intelligent time-domain parameters matching for shock response spectrum and its experimental validation in active vibration control systems", Shock and Vibration **2019**, 2920845 (2019).

[86]M. Musallam and C. M. Johnson, "An efficient implementation of the rainflow counting algorithm for life consumption estimation", IEEE Transactions on reliability **61**, 978–986 (2012).

# Appendices

Appendix A

**Pseudo-algorithm** Below is a compact pseudocode that is easy to translate to any language. It follows the common stack-based implementation: incoming extrema are pushed; whenever the last three extrema meet the cycle-closing criterion a cycle is emitted and the two middle extrema are removed (or adjusted).

**Algorithm 1** Rainflow counting (turning-point / stack algorithm) see [86] and [3]

**Input:** Time-history signal $s[1..N]$
**Output:** List of counted cycles with amplitudes and means
Extract turning points (local maxima/minima) from $s$ and store them in array $T$
Initialize an empty stack $S$
Initialize an empty list $C$ to store counted cycles
**for** each turning point $x$ in $T$ **do**
    Push $x$ onto the stack $S$
    **while** stack $S$ contains at least 3 points **do**
        Let: $X$ = last element of $S$ $Y$ = second last element $Z$ = third last element
        Compute ranges: $R_1 = |Y - Z|$ $R_2 = |X - Y|$
        **if** $R_2 \geq R_1$ **then** ▷ A full cycle is identified
            Form a cycle with range $R_1$
            Compute mean $M = (Z + Y)/2$
            Add $(R_1, M)$ to cycle list $C$
            Remove middle point $Y$ from the stack
        **else**
            **break** ▷ No more cycles can be closed at this step
        **end if**
    **end while**
**end for**
▷ — Process remaining half cycles —
**while** stack $S$ has at least 2 points **do**
    Let $A$ = top point, $B$ = next point
    Half-cycle range $R = |A - B|$
    Mean $M = (A + B)/2$
    Add half-cycle $(R, M)$ to $C$
    Pop $A$ from stack
**end while**
**return** Cycle list $C$